Structural Engineering and Mechanics, Vol. 31, No. 3 (2009) 241-264
DOI: http://dx.doi.org/10.12989/sem.2009.31.3.241

Seismic analysis of transmission towers under various line configurations

Y. H. Lei†

Tamkang University, Department of Software Engineering, Lanyang campus, I-lan County, 26247, Taiwan-ROC

Y. L. Chien

Tamkang University, Civil Engineering Department, Taipei, Taiwan (ROC)

(Received February 27, 2006, Accepted February 18, 2008)

Abstract. In this paper, the dynamic behavior for a group of transmission towers linked together through electrical wires and subjected to a strong ground motion will be investigated in detail. In performing the seismic analysis, the wires and the towers concerned are modeled, respectively, by using the efficient cable elements and the 3-D beam elements both considering geometric nonlinearities. In addition, to enhance the reliability and applicability of analytical outcome, a sophisticated soil-structure interaction model will be utilized in analyses. The strength capacities and the fracture occurrences for the main members of the tower are examined with the employment of the appropriate strength interaction equations. It is expected that by aid of this investigation, those who are engaged in code constitution or in practical designing of transmission towers may gain a better insight into the roles played by the interaction force between towers and wires and by the configurations of transmission lines under strong earthquake.

Keywords: Chi-Chi earthquake; geometric nonlinearity; soil-structure interaction.

1. Introduction

The importance of the transmission tower on economy of nation and living of people has been well recognized. During the attack of the Chi-Chi earthquake, having a size of 7.3 in Richer's magnitude, in Taiwan on Sept. 21, 1999, over two thousand four hundred residents were killed. Besides, the strong vibration of the ground motion has caused the collapse of a pivotal transmission tower located in the central region of the state. As a result, the government was forced to take measures of reducing electricity supply for more than six weeks. During this period, a great inconvenience of living was brought to the people, and a huge commercial loss was incurred in the high-tech industry of the island.

To achieve the aim of distributing electricity everywhere in a country, many transmission towers are hence built in a rugged circumstance with climbing mountains or crossing rivers. Accordingly, the elevation at which some tower structures are located may differ from that associated with other

† Associate Professor, Ph.D., Corresponding author, E-mail: demanad@mail.tku.edu.tw

transmission towers. Moreover, the marching route of the tower procession in such a circumstance may exhibit in an extremely irregular manner. This variation on either the elevation or the orientation of the geometric configuration for a group of transmission towers would certainly affect the interaction force between electrical wires and tower structures.

To achieve the aim of distributing electricity everywhere in a country, many transmission towers are hence built in a rugged circumstance with climbing mountains or crossing rivers. Accordingly, the elevation at which some tower structures are located may differ from that associated with other transmission towers. Moreover, the marching route of the tower procession in such a circumstance may exhibit in an extremely irregular manner. This variation on either the elevation or the orientation of the geometric configuration for a group of transmission towers would certainly affect the interaction force between electrical wires and tower structures.

The conventional seismic analysis of transmission towers is usually undertaken by taking each of towers as an isolated structure without taking the inertia coupling and the strong traction of high-voltage cables lining up in various directions into account. Furthermore, many of structural engineers were used to simply ignore the wire mass or to take it as the lumped-mass affiliated to the tower in seismic analysis. The results obtained by following such analytical schemes would not be able to reflect the actual forced conditions of the tower structure itself as well as the base foundation beneath it.

To describe properly the deformed behavior of the structural joints connecting tower members together is probably one of the most complicated tasks in tower analyses. The complicacies are mainly due to (1) the flexibility of joints behaving nonlinearly from the very onset of loading (AlBermani and Kitipornchai 1993), (2) the joint slippage resulting from the providence of erection tolerance in the course of producing the bolt holes throughout tower members (AlBermani and Kitipornchai 1993, Knight and Santhakumar 1993, Kitipornchai *et al.* 1994) and (3) the flexural deformations of the primary leg member, introduced from the secondary diagonal members jointed with the leg member by using bolted connections (Knight and Santhakumar 1993, AlBermani, and Kitipornchai 2003) Since the transmission tower is usually constructed by using the rolled steel angles which are eccentrically connected one another, nonlinear seismic analysis with respect to such a structure is widely known extremely difficult when the flexural deformations of the angle-section members are intended to be taken into account. In consequence, a proof-loading or full-scale testing combined with a linear elastic analysis in which the assumption of axially loaded conditions is applied to all the component members has formed an integral part of the tower design in practice (AlBermani, and Kitipornchai 2003). To simplify the calculations involved, the effects due to joint flexibility and bolt slippage will be neglected in this paper. It is expected that the adoption of these assumptions would not lessen much the value of the findings regarding the variation tendency of the internal forces acting on the main component members of the towers under various line configurations.

Being slender and tall in appearance, the transmission tower is destined to be susceptible to the effect of geometric nonlinearity. In addition, either the cable mass of the structural system in which transmission towers are spaced over a long distance or the soil-structure interaction, especially for the cases where tower structures are built on the soft ground, would be expected to bring noticeable influences on the dynamic behavior of the tower. In this paper, the cable element, proposed by Desai *et al.*, efficient in describing the dynamic-behavior of electrical wires will be adopted (Desai *et al.* 1995). Besides, in formulation of beam-column elements employed for modeling the tower members, the effect of geometric nonlinearity will be considered. The influence of soil-structure interaction on the seismic responses of transmission towers will be considered by incorporating a sophisticated interaction model proposed by Song and Wolf (1994, 1996, 1997) into the global tower system.

2. Formulation of structural modeling

All seismic analyses in this paper are undertaken with respect to the structural system composed of various portions including electrical wires, tower bodies, near-field soil blocks and end-restraint springs, as indicated in Fig. 1. The formulation involved in the modeling of each portion of the system will be presented in the following.

2.1 Electrical wires and end-restraint springs

Being highly flexible and undergoing significant deformations, the electrical wire ought therefore to be analyzed in the manner of taking the effect of geometric nonlinearity into account. Having not been used in authors' former studies (Lei and Yeh 2003, Lei and Chien 2005) before for describing the dynamic behavior of transmission lines, the 3-node, iso-parametric cable element proposed by Desai, Popplewell and Shah will be adopted in the current study (Desai *et al.* 1995). Consider the cable element referred to the fixed global X, Y, Z coordinates and the initial intrinsic coordinate S, in the manner illustrated in Fig. 2. The elemental nodal displacement vector, $\mathbf{u}_i$, in the global coordinate system is defined as

$$\mathbf{u}_i = (U_1, V_1, W_1, \theta_1, U_2, V_2, W_2, \theta_2, U_3, V_3, W_3, \theta_3) \tag{1}$$

where U_i, V_i, W_i are the translational displacements at node i (i = 1, 2, 3), and θ_i is the rotation about S corresponding to node i. The global coordinates and displacements at any point of the element are given, respectively, by

$$(X, Y, Z) = \sum_{K=1}^{3} N_K(X_K, Y_K, Z_K) \tag{2}$$

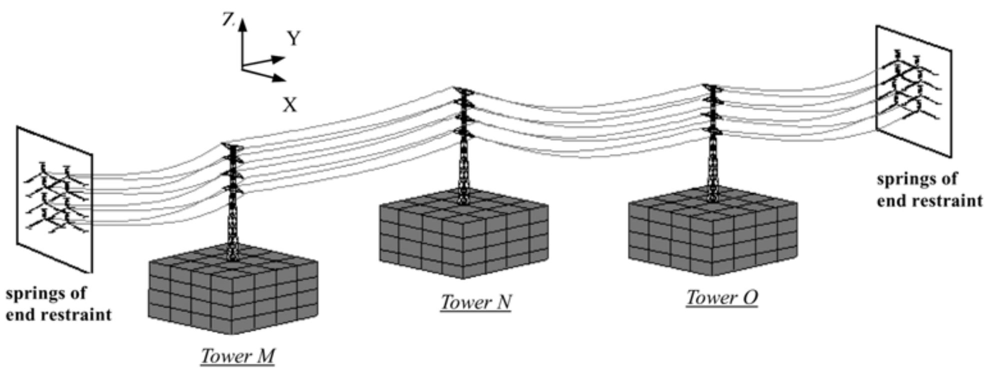

Fig. 1 Analytical model of tower system

and

$$(U, V, W, \theta) = \mathbf{N}\mathbf{u}_i \tag{3}$$

In Eq. (2), X_K, Y_K, Z_K are the global nodal coordinates corresponding to node K, and the parabolic shape functions N_K, are

$$N_1 = 2S^2/L_c^2 - 3S/L_c + 1 \tag{4a}$$

$$N_2 = -4S^2/L_c^2 - 4S/L_c \tag{4b}$$

$$N_3 = 2S^2/L_c^2 - S/L_c \tag{4c}$$

where L_c is the length of the element. Moreover, the shape-function matrix $\mathbf{N}$, in Eq. (3) is

$$\mathbf{N} = (N_1\mathbf{I}_4 \;\; N_2\mathbf{I}_4 \;\; N_3\mathbf{I}_4) \tag{5}$$

in which $\mathbf{I}_4$ is the 4×4 identity matrix. Following the standard finite element procedure, one can obtain the elemental consistent mass matrix in terms of the relation given by

$$\mathbf{M}^e = \int_0^{L_c} \mathbf{N}^T \rho \mathbf{N} dS \tag{6}$$

To account for the geometric deformations of the cable, the elemental stiffness matrix $\mathbf{K}_T^e$ is decomposed into

$$\mathbf{K}_T^e = \mathbf{K}^e + \mathbf{K}_\sigma^e \tag{7}$$

where $\mathbf{K}^e$ and $\mathbf{K}_\sigma^e$ are the elastic and geometric stiffness matrices respectively.

In formulation of $\mathbf{K}^e$, the elemental strain- and stress-vectors, $\boldsymbol{\varepsilon}$ & $\boldsymbol{\sigma}$, are expressed, respectively, in the form of

$$\varepsilon = (\varepsilon_S, \varepsilon_\theta) \tag{8}$$

$$\boldsymbol{\sigma} = \mathbf{D}\boldsymbol{\varepsilon} + \boldsymbol{\sigma}_0 \tag{9}$$

In Eq.(8), ε_S is the Lagrangian strain along S, that is

$$\boldsymbol{\varepsilon}_S = \frac{\partial X}{\partial S}\frac{\partial U}{\partial S} + \frac{\partial Y}{\partial S}\frac{\partial V}{\partial S} + \frac{\partial Z}{\partial S}\frac{\partial W}{\partial S} + \frac{1}{2}\left(\left(\frac{\partial U}{\partial S}\right)^2 + \left(\frac{\partial V}{\partial S}\right)^2 + \left(\frac{\partial W}{\partial S}\right)^2\right) \tag{10}$$

$$\div \frac{\partial X}{\partial S}\frac{\partial U}{\partial S} + \frac{\partial Y}{\partial S}\frac{\partial V}{\partial S} + \frac{\partial Z}{\partial S}\frac{\partial W}{\partial S}$$

As to the torsional strain ε_θ in Eq.(8) is defined as

$$\varepsilon_\theta = \partial\theta/\partial S \tag{11}$$

The elasticity matrix $\mathbf{D}$ and the initial stress vector $\boldsymbol{\sigma}_0$ in Eq. (9) are given, respectively, by

$$\mathbf{D} = \frac{1}{A}\begin{pmatrix} AE & B_T \\ B_T & GJ \end{pmatrix} \tag{12}$$

$$\boldsymbol{\sigma}_0 = \frac{1}{A}(T, M_t) \tag{13}$$

where A, E and GJ are the cross-sectional area, modulus of elasticity and torsional rigidity respectively; T and M_t are the initial static tensional-force and twisting-moment of the element; B_T is an axial-torsional coupling parameter (Desai *et al.* 1988). The strain-displacement relationship matrix **B** taking account of the effect of geometric nonlinearity can be expressed as

$$\mathbf{B} = (\mathbf{B}_1 \;\; \mathbf{B}_2 \;\; \mathbf{B}_3) \tag{14}$$

in which

$$\mathbf{B}_k = \begin{pmatrix} \frac{\partial \mathbf{X}^*}{\partial S}\frac{\partial N_k}{\partial S} & \frac{\partial \mathbf{Y}^*}{\partial S}\frac{\partial N_k}{\partial S} & \frac{\partial \mathbf{Z}^*}{\partial S}\frac{\partial N_k}{\partial S} & 0 \\ 0 & 0 & 0 & \frac{\partial N_k}{\partial S} \end{pmatrix}; \quad k = 1, 2, 3 \tag{15}$$

The superscript * in the above equation refers to the deformed configurations as shown in Fig. 2 and furthermore

$$(X^*, Y^*, Z^*) = (X, Y, Z) + (U, V, W) \tag{16}$$

The elastic stiffness matrix of the element $\mathbf{K}^e$, now can be computed explicitly in the global coordinate system in terms of the relation of

$$\mathbf{K}^e = \int_0^{L_c} A\mathbf{B}^T\mathbf{D}\mathbf{B}dS \tag{17}$$

On the other hand, the geometric stiffness matrix of the element $\mathbf{K}_\sigma^e$, can be derived in the global system as

$$\mathbf{K}_\sigma^e = \int_0^{L_c} \mathbf{G}^T\mathring{\mathbf{S}}\mathbf{G}dS \tag{18}$$

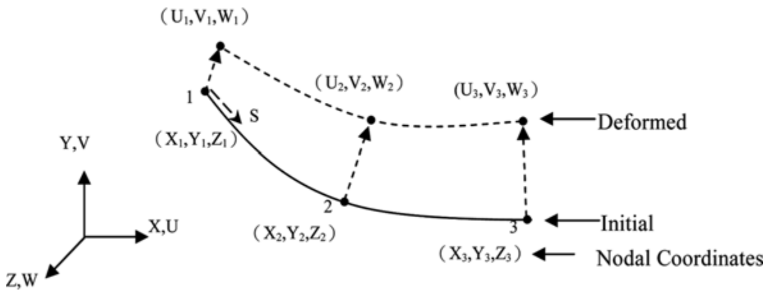

Fig. 2 Deformed configuration for parabolic cable element

where

$$\mathbf{G} = \left(\frac{\partial N_1}{\partial S}\mathbf{I}_4 \;\; \frac{\partial N_2}{\partial S}\mathbf{I}_4 \;\; \frac{\partial N_3}{\partial S}\mathbf{I}_4 \right) \tag{19}$$

$$\tilde{\mathbf{S}} = T\bar{\mathbf{I}} \tag{20}$$

and

$$\bar{\mathbf{I}} = diag(1\ \ 1\ \ 1\ \ 0) \tag{21}$$

The end-restraint springs in Fig. 1 are used for modeling the tensile restraints provided by a series of transmission towers located beyond either end of the system. In the current study, the stiffness of any end-restraint spring placed along certain direction will be chosen as 1.5 times the stiffness for a single tower, measured in the same direction as that of the spring.

2.2 Tower structures

The component members of each transmission tower in the system will be modeled by using 3-D beam-column elements, and the Cartesian coordinate system composed of x-, y- and z-axes as illustrated in Fig. 3 is adopted as the local coordinate system of these elements. As observed in the figure, the longitudinal direction for the element is assumed to be coincident with the x-axis, and the two principal axes perpendicular each other over the cross section are in y- and z-directions respectively. The symbols u_1, u_2 and u_3 represent the translational displacements at the left end of the element in x-, y- and z-directions respectively; u_7, u_8 and u_9 represent the translational displacements at the right end of the element in x-, y- and z-directions respectively; u_4, u_5 and u_6 represent the rotational displacements at the left end of the element around x-, y- and z-axes respectively; u_{10}, u_{12} and u_6 represent the rotational displacements at the right end of the element around x-, y- and z-axes respectively. Besides, the nodal force corresponding to the nodal displacement u_i $(i = 1, 2, \ldots, 12)$ will be denoted by symbol F_i. The stiffness matrix for the element in Fig. 3 can be written as

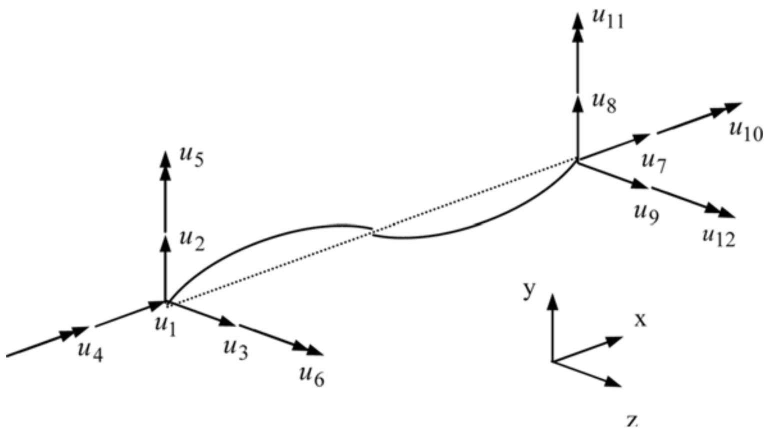

Fig. 3 Nodal displacement of 3-D beam-column element

$$\mathbf{K}_e = \begin{bmatrix} k(1,1) & k(1,2) & \dots & \dots & k(1,12) \\ k(2,1) & k(2,2) & \dots & \dots & k(2,12) \\ \dots & \dots & \dots & \dots & \dots \\ \dots & \dots & \dots & \dots & \dots \\ k(12,1) & k(12,2) & \dots & \dots & k(12,12) \end{bmatrix} \tag{22}$$

With the application of the beam-column approach, the stiffness coefficients $k(i,j)$ (i, $j = 1, 2, \dots, 12$), which take account of the effects of geometric nonlinearity, can be derived as follows

$$k(1,1) = k(7,7) = -k(1,7) = (EA/L_e)R \tag{23}$$

$$k(2,2) = k(8,8) = -k(2,8) = (EI_z/L_e^3)S_{1z} \tag{24}$$

$$k(2,6) = k(2,12) = -k(6,8) = -k(8,12) = -(EI_z/L_e^2)S_{2z} \tag{25}$$

$$k(3,5) = k(3,11) = -k(5,9) = -k(9,11) = -(EI_y/L_e^2)S_{2y} \tag{26}$$

$$k(4,4) = k(10,10) = -k(4,10) = GJ/L_e \tag{27}$$

$$k(5,5) = k(11,11) = (EI_y/L_e)S_{3y} \tag{28}$$

$$k(6,6) = k(12,12) = (EI_z/L_e)S_{3z} \tag{29}$$

$$k(5,11) = (EI_y/L_e)S_{4y} \tag{30}$$

$$k(6,12) = (EI_z/L_e)S_{4z} \tag{31}$$

where E is the modulus of elasticity; A and L_e are the cross-sectional area and the length of the beam-column element respectively; I_y and I_z are the moments of inertia corresponding to y- and z-axes respectively; J is the polar moment of inertia; G is the shear modulus of elasticity; R_t is the axial stiffness coefficient used for taking account of the bowing effect, that is the axial-deformation effect caused by flexural force. The stability functions S_{jy} and S_{jz} ($j = 1, 2, 3, 4$) in the above equations, used for taking the effect of the interaction between axial and flexural forces into consideration, can be derived as

(i) When the internal axial force is in compression ($F_1 = -F_7 > 0$):

$$S_{1y} = \frac{\hat{\phi}_y^3 \sin\hat{\phi}_y}{(2 - 2\cos\hat{\phi}_y - \hat{\phi}_y \sin\hat{\phi}_y)} \tag{32}$$

$$S_{2y} = \frac{\hat{\phi}_y^3 (1 - \cos\hat{\phi}_y)}{(2 - 2\cos\hat{\phi}_y - \hat{\phi}_y \sin\hat{\phi}_y)} \tag{33}$$

$$S_{3y} = \frac{\hat{\phi}_y (\sin\hat{\phi}_y - \hat{\phi}_y \cos\hat{\phi}_y)}{(2 - 2\cos\hat{\phi}_y - \hat{\phi}_y \sin\hat{\phi}_y)} \tag{34}$$

$$S_{4y} = \frac{\hat{\phi}_y (\hat{\phi}_y - \hat{\phi}_y \sin\hat{\phi}_y)}{(2 - 2\cos\hat{\phi}_y - \hat{\phi}_y \sin\hat{\phi}_y)} \tag{35}$$

in which

$$\hat{\phi}_y = \sqrt{PL^2/EL_y} \tag{36}$$

(ii) When the internal axial force is in tension ($F_1 = -F_7 < 0$):

$$S_{1y} = \frac{\hat{\phi}_y^3 \sinh\hat{\phi}_y}{(2-2\cosh\hat{\phi}_y + \hat{\phi}_y \sinh\hat{\phi}_y)} \tag{37}$$

$$S_{2y} = \frac{\hat{\phi}_y^3(\cosh\hat{\phi}_y - 1)}{(2-2\cosh\hat{\phi}_y + \hat{\phi}_y \sinh\hat{\phi}_y)} \tag{38}$$

$$S_{3y} = \frac{\hat{\phi}_y(\hat{\phi}_y \cosh\hat{\phi}_y - \sinh\hat{\phi}_y)}{(2-2\cosh\hat{\phi}_y + \hat{\phi}_y \sinh\hat{\phi}_y)} \tag{39}$$

$$S_{4y} = \frac{\hat{\phi}_y(\hat{\phi}_y \sinh\hat{\phi}_y - \hat{\phi}_y)}{(2-2\cosh\hat{\phi}_y + \hat{\phi}_y \sinh\hat{\phi}_y)} \tag{40}$$

Replacing I_y in Eqs. (32)-(35) & (37)-(40) with I_z leads to the shifting for the quantities on the left-hand side of these equations from S_{jy} ($j = 1, 2, 3, 4$) to S_{jz}. In undertaking the seismic time-history analysis, Newton-Raphson method will be adopted as the iterative scheme for modifying the stiffness coefficients in Eqs. (23)-(31) repeatedly at each time step until the convergence is attained.

2.3 Soil-structure interaction

Since the seismic responses of the transmission tower is closely related to the properties of the soil in the vicinity of the tower base, it would be essentially required to take the soil-structure interaction into consideration for obtaining satisfactory results. According to the method of consistent infinitesimal finite-element cell (Wolf and Song 1994, 1996, 1997), there exists a layer of finite-element cell between the borders of near-field and far-field soils. The interfaces at both interior and exterior boundaries of the finite-element cell are assumed geometrically similar with each other, and the thickness of the cell h_c is assumed to be given by (referring to Fig. 4)

$$h_c = r_e - r_i \tag{41}$$

Recognizing that h_c represents the quantity with infinitesimal magnitude, one can derive the stiffness matrix of the cell, $\mathbf{K}^*$, by following the standard finite-element procedures without difficulty. By denoting the interaction force acting on near-field soil as $\mathbf{q}(t)$, the equations of motion in the matrix form, for the system consisting of superstructure and near-field soil, can thus be expressed as

$$\mathbf{M}\ddot{\mathbf{u}}(t) + \mathbf{C}\dot{\mathbf{u}}(t) + \mathbf{K}\mathbf{u}(t) = -\mathbf{M}\tilde{\mathbf{i}}\ddot{u}_g(t) + \mathbf{q}(t) \tag{42}$$

where $\mathbf{M}$, $\mathbf{C}$ and $\mathbf{K}$ are the mass, damping and stiffness matrices of the system respectively; $\mathbf{u}(t)$ and $\ddot{u}_g(t)$ are displacement-response vector and ground acceleration respectively; $\mathbf{i}$ is the pseudo-static displacement vector of the system. Denoting the interaction force acting on far-field soil by

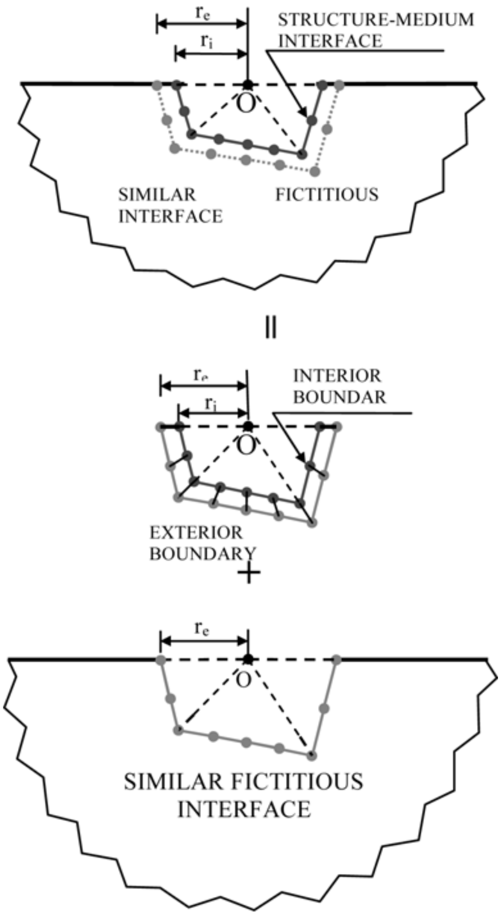

Fig. 4 Infinitesimal finite-element cell and similar fictitious interface

using the symbol $\mathbf{r}(t)$ leads to

$$\mathbf{q}(t) = -\mathbf{r}(t) \tag{43}$$

The force-displacement relationship of the far-field soil can be written in the frequency domain as

$$\mathbf{r}(\omega) = \mathbf{S}^{\infty}(\omega)\mathbf{u}(\omega) \tag{44}$$

in which $\mathbf{S}^{\infty}(\omega)$ is the dynamic stiffness matrix and the superscript ∞ is used to denote the unbounded nature of far-field soil. If $\mathbf{S}^{\infty}(t)$ is the inverse Fourier transform of $\mathbf{S}^{\infty}(\omega)$, then $\mathbf{r}(t)$ is given by

$$\mathbf{r}(t) = \int_0^t \mathbf{S}^{\infty}(t-\tau)\mathbf{u}(\tau)d\tau \tag{45}$$

The mass matrix $\mathbf{M}^{\infty}(\omega)$ corresponding to dynamic-stiffness matrix $\mathbf{S}^{\infty}(\omega)$ in frequency domain can be expressed as

$$\mathbf{M}^{\infty}(\omega) = \mathbf{S}^{\infty}(\omega)/(i\omega)^2 \tag{46}$$

By applying the above relation, Eq. (45) is now able to be written in an alternate form as

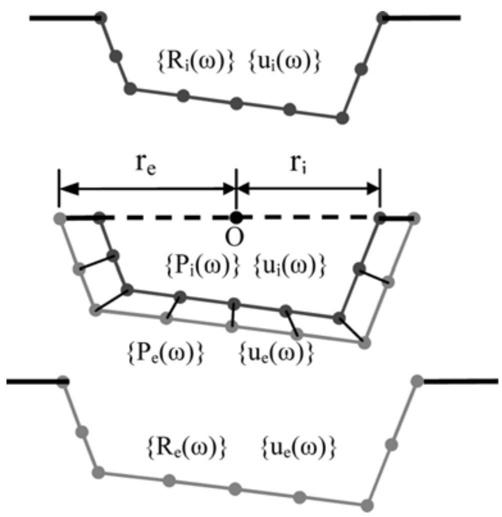

Fig. 5 Nodal forces of finite-element cell and interaction forces at interior and exterior boundaries

$$\mathbf{r}(t) = \int_0^t \mathbf{M}^{\infty}(t-\tau)\ddot{\mathbf{u}}(\tau)d\tau \tag{47}$$

in which $\mathbf{M}^{\infty}(t)$ is usually called the acceleration unit-impulse response matrix. The force-displacement relationship of the finite-element cell located between the interior and exterior boundaries is given by (referring to Fig. 5)

$$\mathbf{S}(\omega)\mathbf{u}(\omega) = \mathbf{p}(\omega) \tag{48}$$

Partitioning the degrees of freedom into those corresponding to interior and exterior boundaries separately yields

$$\begin{pmatrix} \mathbf{S}_{ii}(\omega) & \mathbf{S}_{ie}(\omega) \\ \mathbf{S}_{ei}(\omega) & \mathbf{S}_{ee}(\omega) \end{pmatrix} \begin{pmatrix} \mathbf{u}_i(\omega) \\ \mathbf{u}_e(\omega) \end{pmatrix} = \begin{pmatrix} \mathbf{p}_i(\omega) \\ \mathbf{p}_e(\omega) \end{pmatrix} \tag{49}$$

in which the subscripts i and e are used to denote the conditions associated with interior and exterior boundaries respectively. Evidently, the nodal forces of the finite-element cell and the interaction force acting on the far-field soil would be related to each other as expressed by

$$\mathbf{p}_i(\omega) = \mathbf{r}_i(\omega) \tag{50}$$

$$\mathbf{p}_e(\omega) = -\mathbf{r}_e(\omega) \tag{51}$$

in which $\mathbf{r}_i(\omega)$ and $\mathbf{r}_e(\omega)$ are given, respectively, by

$$\mathbf{r}_i(\omega) = \mathbf{S}_i^{\infty}(\omega)\mathbf{u}_i(\omega) \tag{52}$$

$$\mathbf{r}_e(\omega) = \mathbf{S}_e^{\infty}(\omega)\mathbf{u}_e(\omega) \tag{53}$$

By making use of Eqs. (50)-(53), Eq. (49) can then be rewritten as

$$\begin{pmatrix} \mathbf{S}_{ii}(\omega) & \mathbf{S}_{ie}(\omega) \\ \mathbf{S}_{ei}(\omega) & \mathbf{S}_{ee}(\omega) \end{pmatrix} \begin{pmatrix} \mathbf{u}_i(\omega) \\ \mathbf{u}_e(\omega) \end{pmatrix} = \begin{pmatrix} \mathbf{S}_i^{\infty}(\omega) & \mathbf{0} \\ \mathbf{0} & -\mathbf{S}_e^{\infty}(\omega) \end{pmatrix} \begin{pmatrix} \mathbf{u}_i(\omega) \\ \mathbf{u}_e(\omega) \end{pmatrix} \tag{54}$$

The governing equations for the finite-element cell in frequency domain can be derived from Eq. (54) by applying the assumption of infinitesimal cell thickness and by making use of the relation of

$$\mathbf{S}(\omega) = \mathbf{K}^* - \omega^2 \mathbf{M}^* \tag{55}$$

in which $\mathbf{M}^*$ is the mass matrix of the finite-element cell. Performing the algorithm of inverse Fourier transformation for obtaining the governing equations in time domain first, and then discretizing this domain afterward, one would obtain the acceleration unit-impulse response $\mathbf{M}^{\infty}(t)_{,n}$ $(n = 1, 2, \ldots, N)$ corresponding to the nth time step. With the use of the assumption of uniform variation in acceleration within time interval Δt, Eq. (47) can be rewritten as

$$\mathbf{r}(t) = \mathbf{M}'\ddot{\mathbf{u}}(t) + \mathbf{f}'(t) \tag{56}$$

in which

$$\mathbf{M}' = \frac{\Delta t}{2}\mathbf{M}^{\infty}{}_{,1} \tag{57}$$

$$\mathbf{f}'(t) = \frac{\Delta t}{2}\sum_{n=2}^{N}\mathbf{M}^{\infty}{}_{,n}\ddot{\mathbf{u}}((N-n)\Delta t) + \ddot{\mathbf{u}}((N-n+1)\Delta t) + \frac{\Delta t}{2}\mathbf{M}^{\infty}{}_{,1}\mathbf{u}((N-1)\Delta t) \tag{58}$$

Accordingly, the equations of motion in Eq. (42) can be expressed by

$$(\mathbf{M} + \mathbf{M}')\ddot{\mathbf{u}}(t) + \mathbf{C}\dot{\mathbf{u}}(t) + \mathbf{K}\mathbf{u}(t) = -\mathbf{M}\tilde{\mathbf{i}}\ddot{u}_g(t) - \mathbf{f}'(t) \tag{59}$$

3. Failure index

It is recognized that the fracture of beam-column members is not purely caused by a single type of internal force but by the combined action of several kinds of internal forces including axial, flexural, shear and perhaps torsional forces in usual. According to the investigation undertaken by Kitipornchai, Zhu, Xiang and Al-Bermani, the yield criterion of beam-column elements in angle sections behaving in an elastic-perfectly manner can be defined as Kitipornchai *et al.* (1988)

$$\tilde{\Phi}(p, m_x, m_y) = \frac{4}{27}\tilde{\lambda}^3(\tilde{\xi} - 1) + (\tilde{\Omega} + \tilde{\mu})^3 sign(1, p) - 3(\tilde{\Omega} + \tilde{\mu})\left(\frac{\tilde{\phi}}{\tilde{\gamma}}\right)^2 sign(1, p)$$
$$+ \tilde{\lambda}(\tilde{\Omega} + \tilde{\mu})^2 + \tilde{\lambda}\left(\frac{\tilde{\phi}}{\tilde{\gamma}}\right)^2 = 0 \tag{60}$$

where

$$\tilde{\Omega} = 0.7071(m_x + \tilde{\alpha}m_y + \tilde{\beta}) \tag{61}$$

$$\tilde{\phi} = 0.7071(-m_x - \tilde{\alpha}m_y + \tilde{\beta}) \tag{62}$$

$$\tilde{\alpha} = 0.7279 + 0.1038|p| + 6.64667p^2 - 13.6904|p|^3 + 7.0038p^4 - 0.03586\sin(2\pi|p|) + 0.1554\cos(2\pi p) \tag{63}$$

$$\tilde{\beta} = -0.04262 - 0.4450|p| + 3.07857p^2 - 3.6351|p|^3 + 1.0002p^4 - 0.06855\sin(2\pi|p|) + 0.04262\cos(2\pi p) \tag{64}$$

$$\tilde{\gamma} = 1.61772 - 0.5039|p| + 2.8671p^2 - 2.6321|p|^3 - 0.00476p^4 + 0.06688\sin(2\pi|p|) + 0.05107\cos(2\pi p) \tag{65}$$

$$\tilde{\xi} = 1.5186 - 1.9165|p| - 16.3988p^2 + 42.0945|p|^3 - 23.8371p^4 + 0.3236\sin(2\pi|p|) - 0.5536\cos(2\pi p) \tag{66}$$

$$\tilde{\lambda} = 1.2 + 8.395(0.9 - |p|)^2 \tag{67}$$

$$\tilde{\mu} = -0.009195 + 0.3133|p| - 1.8183p^2 + 1.4675|p|^3 + 0.0455p^4 - 0.07293\sin(2\pi|p|) + 0.00919\cos(2\pi p) \tag{68}$$

In the above equations, the dimensionless parameters, p, m_y and m_z, are defined, respectively, as

$$p = P/P_y; \quad m_y = M_y/M_{py}; \quad m_z = M_z/M_{pz} \tag{69}$$

where P is the axial force (negative for compressive force); M_y and M_z are the flexural loads around

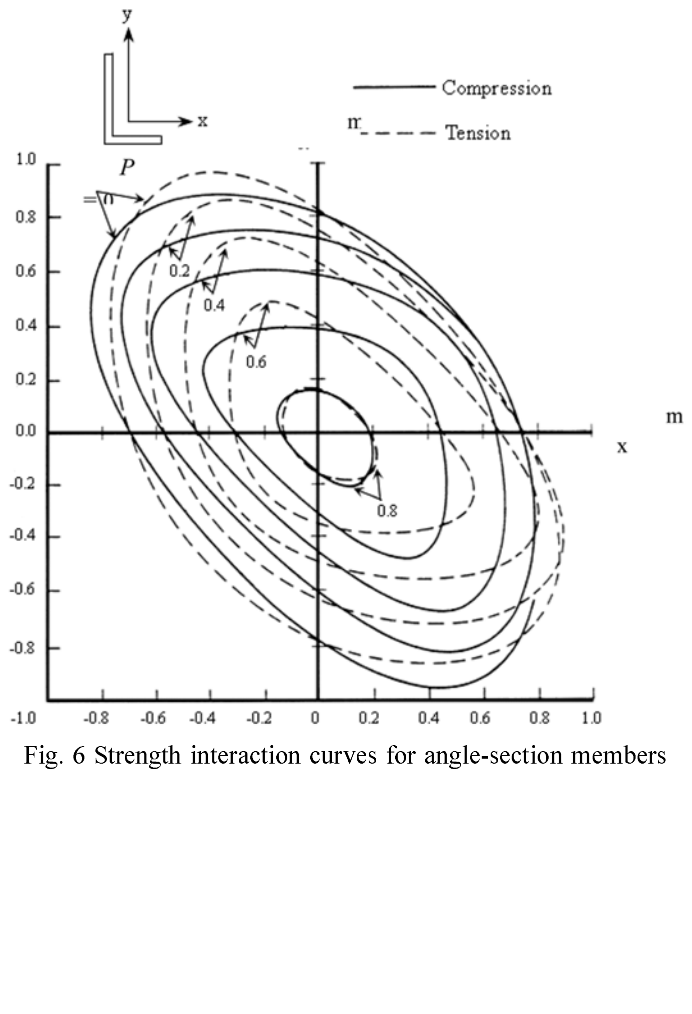

Fig. 6 Strength interaction curves for angle-section members

the local y- and z-axes of the angle element respectively; P_y is the axial yielding strength; M_{py} and M_{pz} are the ultimate plastic moments around the y- and z-axes respectively. In deriving the Eq. (60), a normality condition to the flow rule in plastic analysis has been employed and the shear influence on yielding is ignored. The interaction curves of strength corresponding to prescribed values of p are illustrated in Fig. 6.

Since the global failure of the transmission tower can be triggered by the fracture of any single main leg in the structure, the term "failure index" will be designated to Λ, which is the parameter assumed following the relation given by

$$\log\Lambda = \tilde{\Phi} \tag{70}$$

Accordingly, for the cases where the failure index Λ is smaller than 1, an elastic stress state exits, whereas when the index corresponding to any section of the beam-column element reaches to unity, the fracture of the member occurs.

4. Numerical examples and discussion

The acceleration records of Chi-Chi earthquake measured at TCU084 station in Taichung, Taiwan, having a peak value of 1.00834(g) and the Fourier spectrum as shown in Fig. 7 is taken as the ground excitation. As indicated in Fig. 1, each of the structural systems investigated in the following will contain three tower structures, among which the towers M and N are located on sides, and the tower O in the middle of the system. The distance between adjacent towers is chosen to be 200 meters. Fig. 8 shows the structural pattern for each tower in the system. The electrical wires suspending between two towers is prescribed by a sag-span ratio of 5% and will be modeled by using 20 cable elements aforementioned. Besides, to investigate the effects of soil-structure interaction, various properties of soil, denoted as soil type I, soil type II and soil type III, having the values of modulus of elasticity 6×10^7, 1.2×10^8 and 1.8×10^8 N/m^2 respectively, will be utilized. Each type of soils is assumed having a Poisson's ratio of 0.35 and a mass density of 1800 (kg/m^3). Tables 1

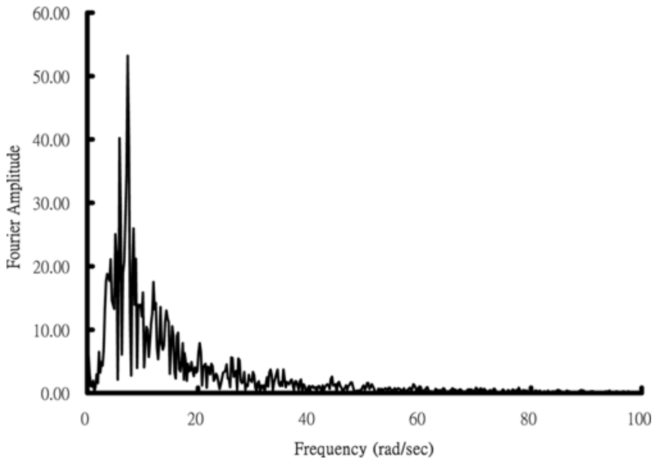

Fig. 7 Fourier spectrum of earthquake acceleration

Table 1 sectional properties of tower members

Sectional Parameter	Segment I		Segment II		Segment III	
	Leg Member	Diagonal Member	Leg Member	Diagonal Member	Leg Member	Diagonal Member
Angle Type (mm)	L 250×30	L 120×10	L 175×15	L 100×10	L 130×10	L 90×10
A (10^{-3} m^2)	14.1	2.3	5.03	1.9	2.5	1.7
E (10^{10} N/m^2)	20	20	20	20	20	20
G (10^{10} N/m^2)	7.69	7.69	7.69	7.69	7.69	7.69
ρ (kg /m^3)	7,850	7,850	7,850	7,850	7,850	7,850
I_y or I_z (10^{-6} m^4)	82	3.19	14.8	1.8	4.09	1.29
J (10^{-8} m^4)	423	7.67	37.7	6.33	8.33	5.67
R_y or R_z (10^{-2} m)	7.63	3.72	5.42	3.08	4.04	2.76
P_y (10^{-5} N/m^2)	4.09	66.7	1.46	55.1	72.5	49.3
M_{py} or M_{pz} (10^{-4} N-m)	2.71	21.6	68.7	14.7	25.5	11.9

Table 2 Sectional properties of wires and piles

Sectional Parameter	Piles (F)	Conduct Wire	Ground Wire
A (m^2)	0.283	4.69×10^{-4}	1.59×10^{-4}
E (N/m^2)	2.46×10^{10}	8.9×10^{4}	1.05×10^{5}
G (N/m^2)	9.47×10^{9}		
ρ (kg /m^3)	2,400		
I_y or I_z (m^4)	6.362×10^{-3}		
J (m^4)	1.272×10^{-2}		
μ (kg /m)		1.628	1.062

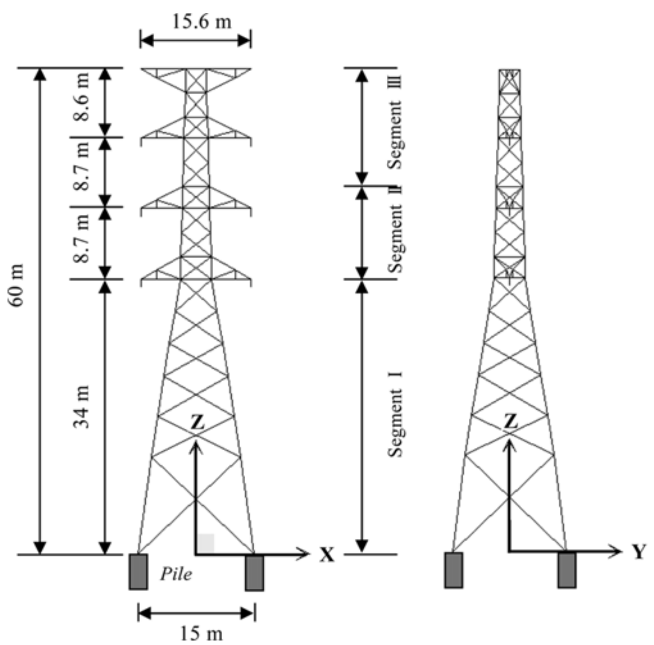

Fig. 8 Structural pattern of transmission tower

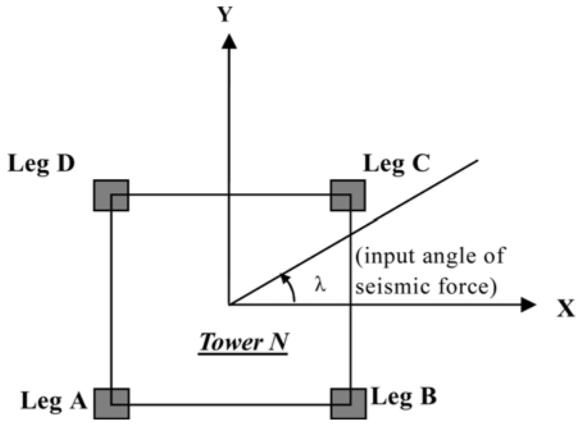

Fig. 9 Base legs and input angle of seismic force

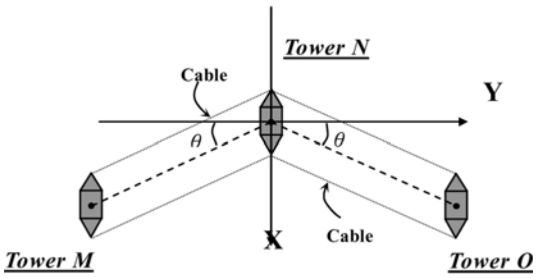

Fig. 10 Description of line angle θ

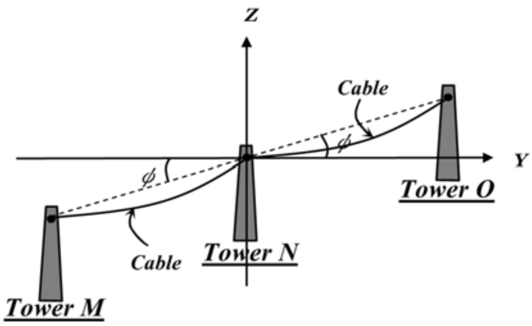

Fig. 11 Description of line angle ϕ

and 2 specify the cross-sectional properties of tower members and of wires and piles respectively.

For simplification of calculations, the investigation to internal-force variation will be mainly focused upon the four leg-members, denoted as Leg A, Leg B, Leg C and Leg D respectively (referring to Fig. 9), located at the lowest portion of tower N. Furthermore, in order to investigate the load effects corresponding to various orientations of ground motion, the term "input angle of seismic force", denoted by using the symbol λ, is defined as the angle of seismic force, measured counterclockwise from the positive direction of X-axis, as illustrated in Fig. 9. In actual calculation, λ will range from zero to 180 degrees with the angle increment of 15 degrees. The positions of tower N relative to towers M and O in both horizontal and vertical directions will be described by using the parameters θ and ϕ respectively, as illustrated in Figs. 10 and 11.

4.1 Variation of Λ due to θ or ϕ

In the condition of $\phi = 0^{\circ}$, the line passing through the base center of towers M, N and O would lie on the XY-plane and be symmetric with respect to the X-axis (referring to Fig. 10), so the variation of failure index, Λ, with the input angle of seismic force, λ, will be investigated for Legs C and D only as shown in Figs. 12 and 13. On the other hand, in the condition of $\theta = 0^{\circ}$, the values of Λ corresponding to $\lambda = \lambda^{*}$ for Legs A and C would be equal to those corresponding to $\lambda = \pi$ -

λ^* for Legs B and D respectively (referring to Figs. 9-11), so the variation of Λ with λ will be investigated for Legs B and C only as shown in Figs. 14 and 15.

Two phenomena will be easily found by observing Figs. 12-15 as follows: (1) The peak values of Λ would usually occur at the time when the seismic force acts in the direction parallel to the tower-base diagonals, which pass through Legs A and C at $\lambda = 45^{\circ}$ and through Legs B and D at $\lambda = 135^{\circ}$, respectively. (2) The larger the value of θ or ϕ is the larger Λ will usually be. In addition, it

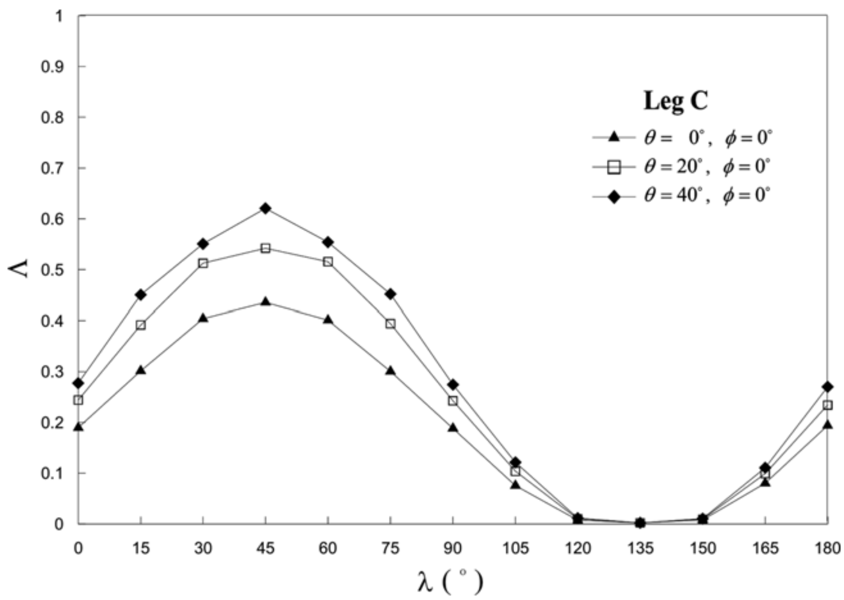

Fig. 12 Failure index of Leg C with $\phi = 0^{\circ}$ under varied θ

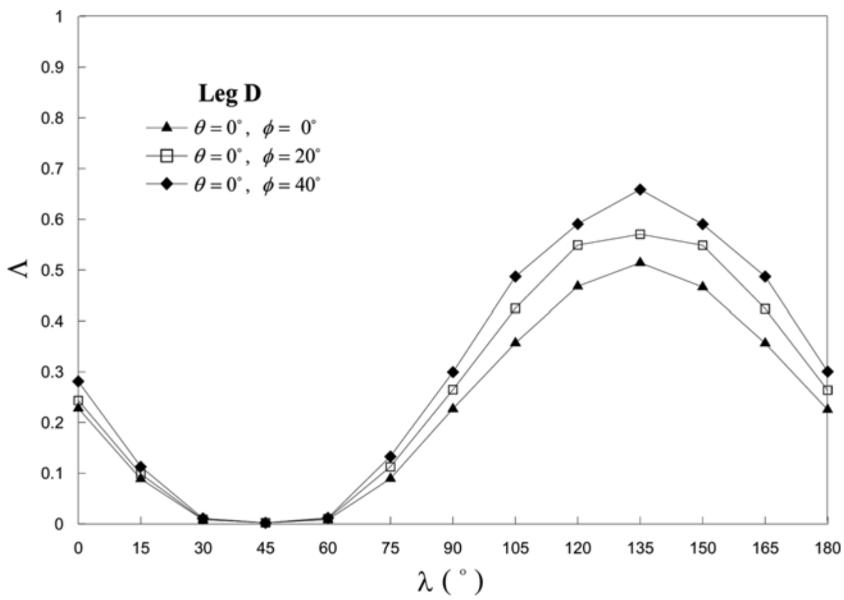

Fig. 13 Failure index of Leg D with $\theta = 0^{\circ}$ under varied ϕ

can be found by making the comparison between Fig. 12 and Fig. 15 that under any fixed value of λ, the values of Λ corresponding to the cases where transmission-line configurations vary in horizontal plane only would be somewhat larger than those in vertical plane only. This implies that the extent of strength reduction for tower main-legs due to θ is usually more significant than that due to ϕ.

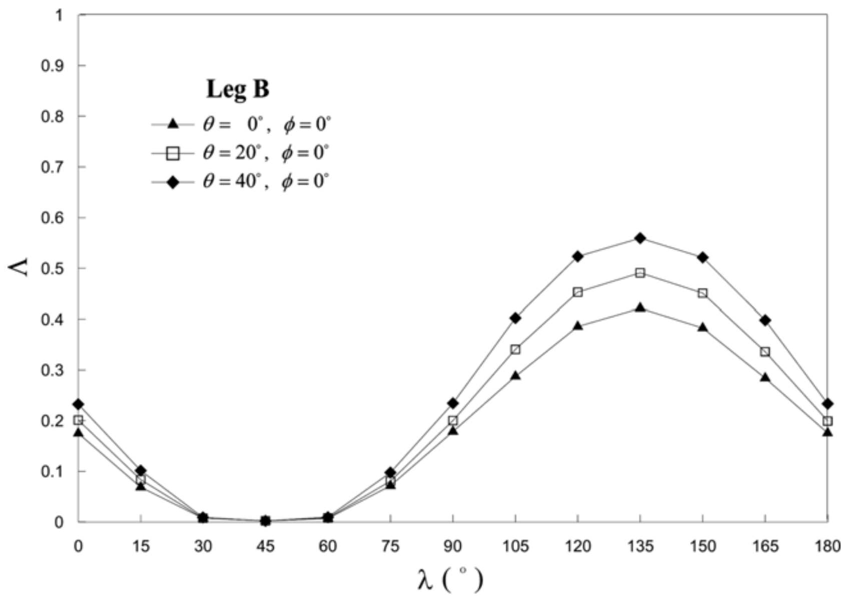

Fig. 14 Failure index of Leg B with $\phi = 0^{\circ}$ under varied θ

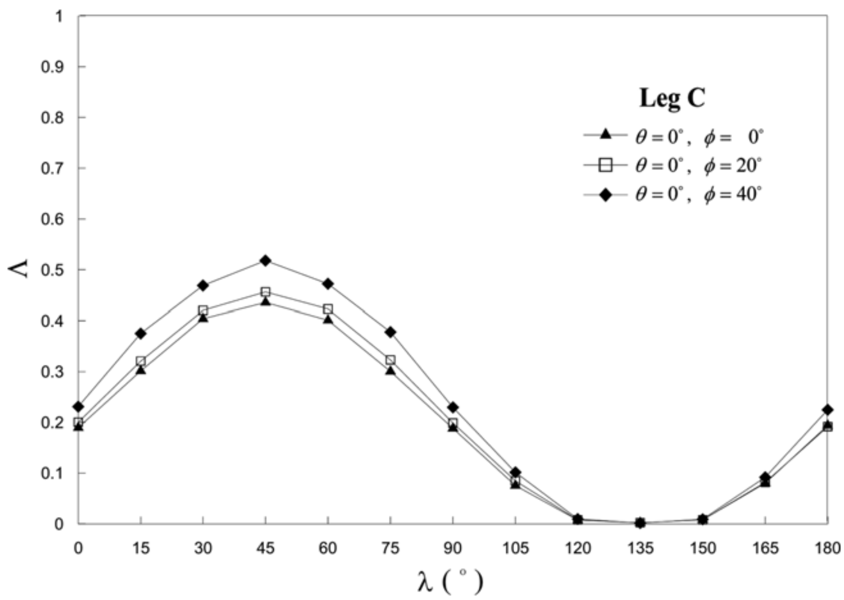

Fig. 15 Failure index of Leg C with $\theta = 0^{\circ}$ under varied ϕ

4.2 Cable-mass participation in responses

The electrical wires connected with transmission towers and lining up in the air over a large span, although possessing pretty low rigidity, are usually expected making a significant contribution to the seismic responses of tower members mainly due to the large quantities of cable mass. Figs. 16, 17 and 18 show the variation of Λ corresponding to the cases of all cable effects being excluded, cable

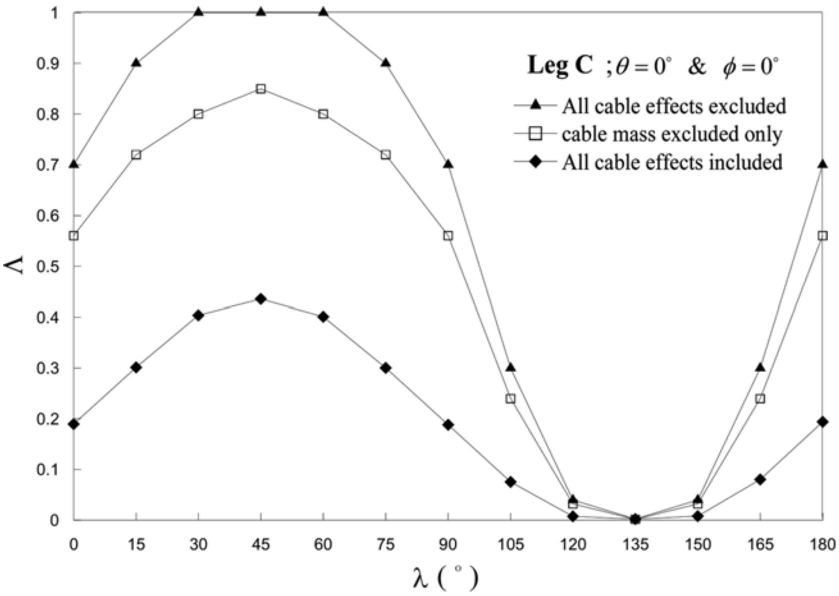

Fig. 16 Failure index considering cable-mass effect with $\theta = \phi = 0^o$

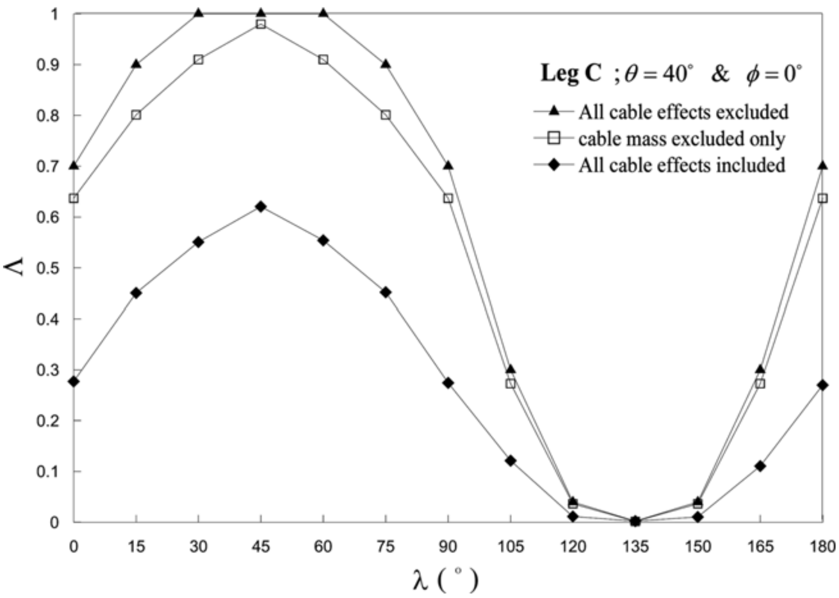

Fig. 17 Failure index considering cable-mass effect with $\theta = 40^o$ & $\phi = 0^o$

mass being excluded only and all cable effects being included respectively. It is shown in all figures that in comparison with the cable stiffness, the cable mass would affect the internal forces for the tower member more significantly. This is because that the existence of cable mass leads to the shifting of the fundamental frequency for the structural system considered, from the value lower than the peak frequency of the earthquake (about 7.3 rad/sec as indicated in Fig. 7) to that even much lower. As a consequence, one might agree that cable-mass participation in total responses is

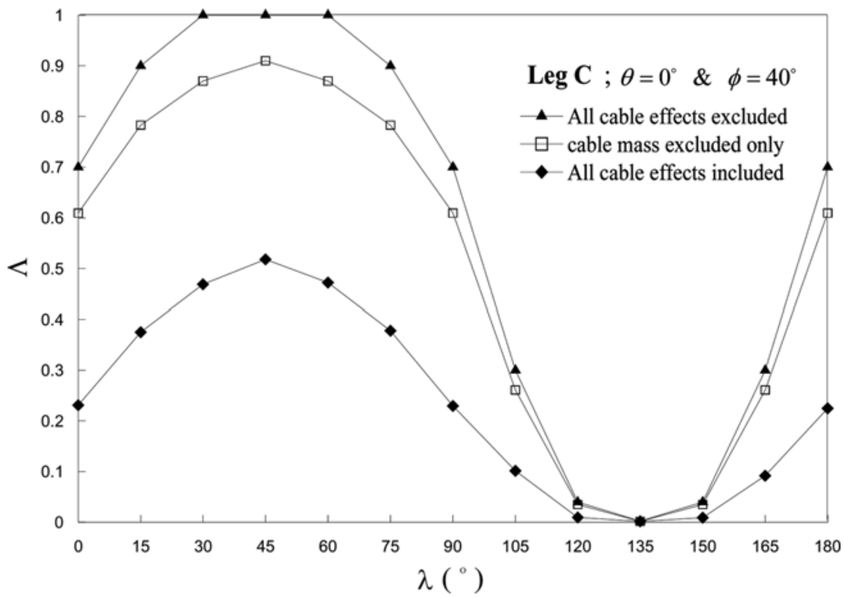

Fig. 18 Failure index considering cable-mass effect with $\theta = 0^o$ & $\phi = 40^o$

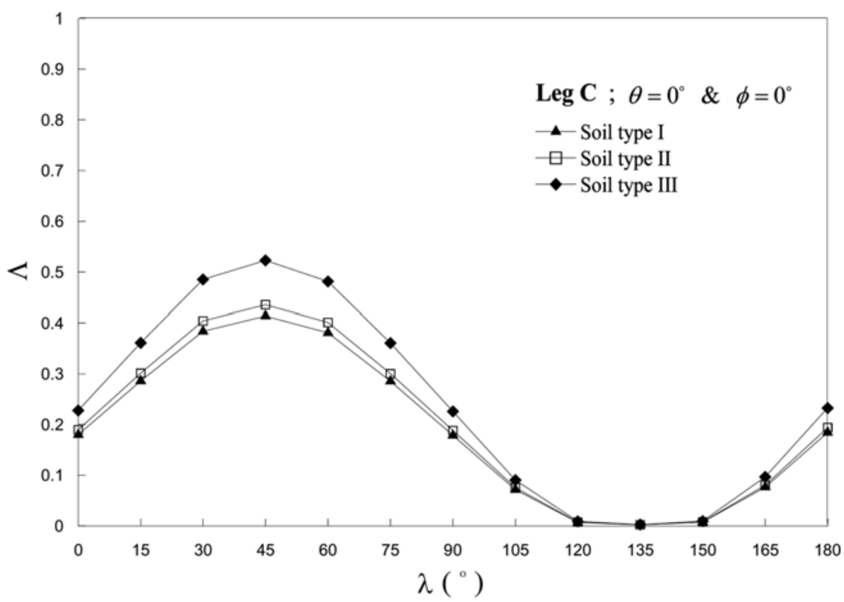

Fig. 19 Failure index with $\theta = \phi = 0^o$ under various soil properties

one of the most important and intriguing themes in seismic analyses of transmission-tower systems.

4.3 Variation of Λ due to soil properties

Although it would be usually more efficient to solve the soil-structure interaction problem in frequency domain than in time domain, this is, however, not applicable to the cases where the

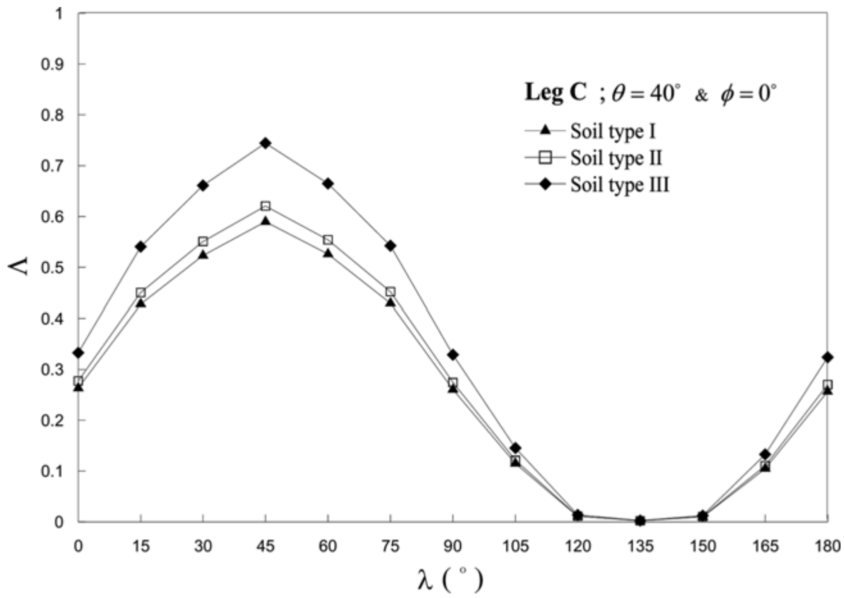

Fig. 20 Failure index with $\theta = 40^o$ & $\phi = 0^o$ under various soil properties

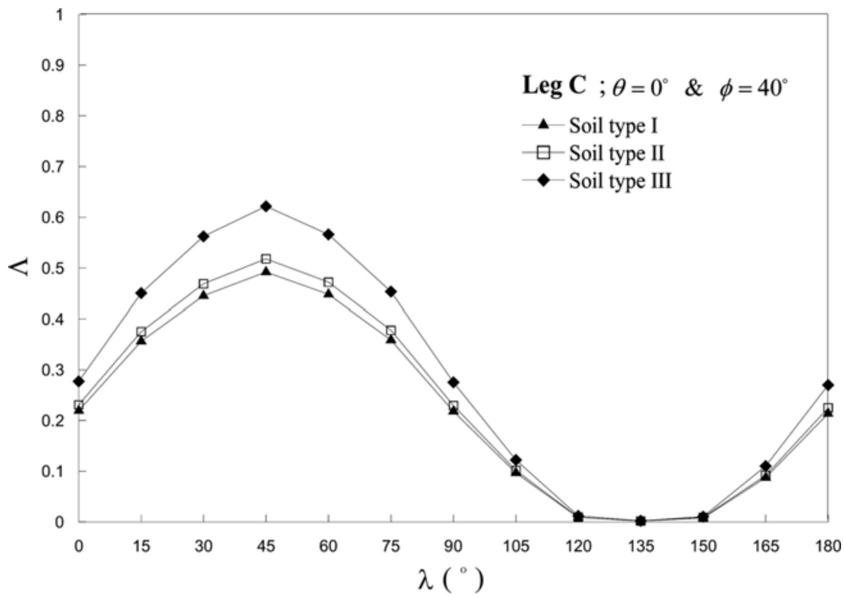

Fig. 21 Failure index with $\theta = 0^o$ & $\phi = 40^o$ under various soil properties

geometric-nonlinearity effect of the structure is intended to be taken into account. The reason is due to the fact that the iteration algorithm utilized in nonlinear analysis can be effectively implemented in time domain only. The aforementioned "method of consistent infinitesimal finite-element cell", since being derived in time domain, would be appropriate to the current study for investigating the effect of soil-structure interaction. Figs. 19-21 show the variation of λ corresponding to soil types I, II and III, under various line configurations respectively. It is observed that the stiffer the soil

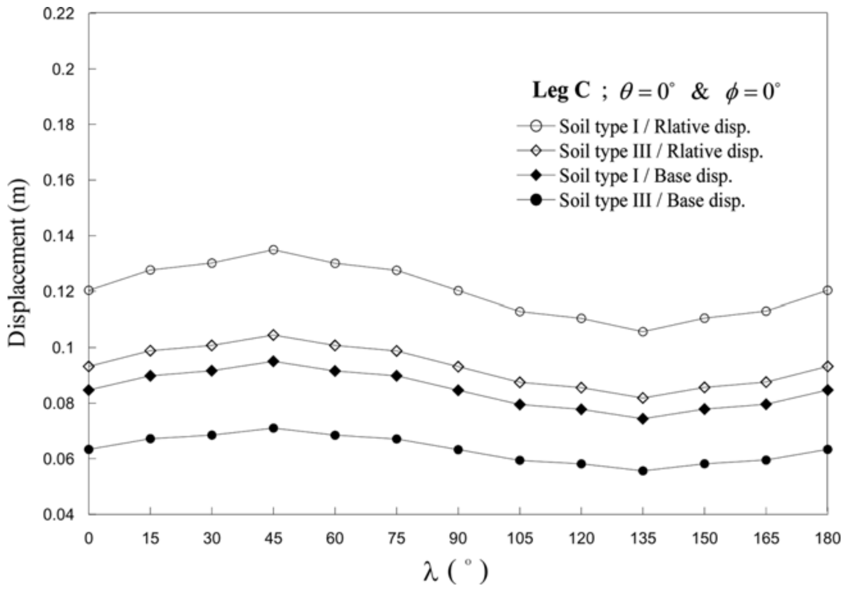

Fig. 22 Base and relative disps. with $\theta = \phi = 0^{\circ}$ under various soil properties

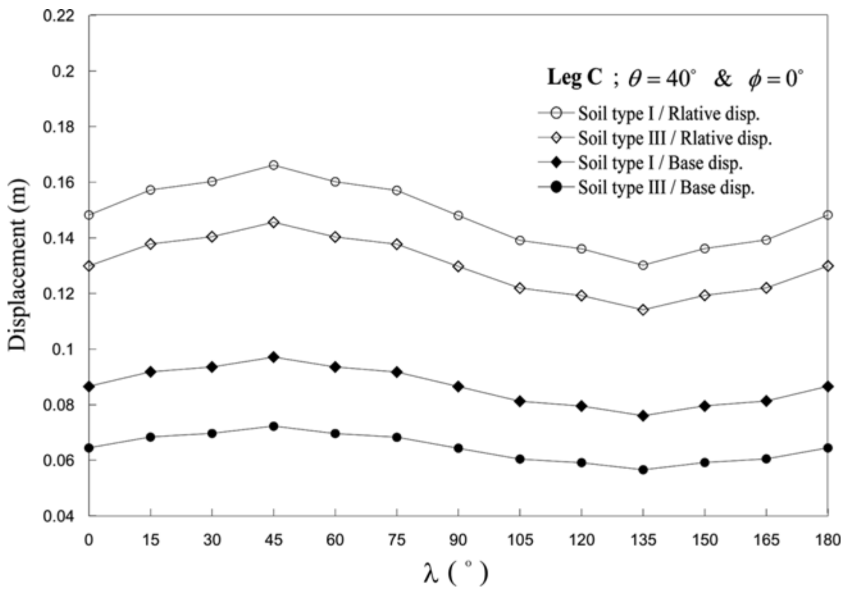

Fig. 23 Base and relative disps. with $\theta = 40^{\circ}$ & $\phi = 0^{\circ}$ under various soil properties

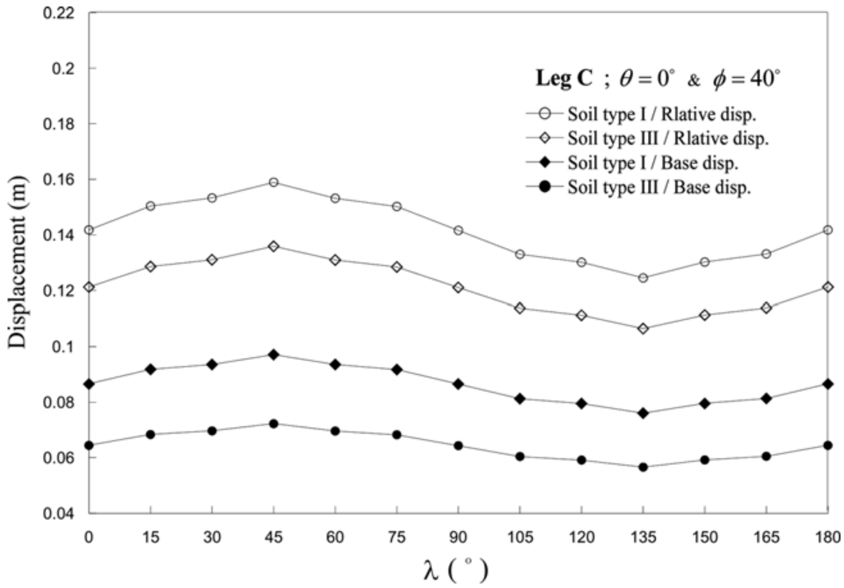

Fig. 24 Base and relative disps. with $\theta = 0^\circ$ & $\phi = 40^\circ$ under various soil properties

surrounding the base of the tower is the higher Λ will usually be. Moreover, to make a further investigation into the structural behavior due to soil properties, both the absolute displacements at the bottom of Leg C and the displacements at the top relative to those at the bottom of the same member corresponding to various types of soil are illustrated in Figs. 22-24. Although larger absolute displacements will usually be found at the bottom of the main leg for the cases with softer soil, the values of Λ are, however, larger with stiffer soil. In other words, the variation tendencies of Λ corresponding to various soil properties are similar to those of the relative displacement at the top but not of the absolute displacement at the bottom of the main member.

5. Conclusions

Having undertaken the seismic analysis in consideration of the effect of geometric nonlinearity, with respect to the structural system modeled by using efficient cable elements, beam-column elements, end-restraint elements and the infinitesimal finite-element cell associated with soil-structural interaction, one may learn that the ignorance of cable contribution to total seismic responses, especially the portion caused by the cable mass, would induce significant errors in predicting the ultimate strength of tower members.

The larger the value of θ or ϕ is the larger Λ will usually be. In the condition of either varied θ or ϕ, the peak value of failure index for any main leg-member would usually occur at the time when the seismic force acts in the direction parallel to the tower-base diagonals passing through the main leg-members considered. Furthermore, it is found that under any fixed value of input angle of seismic angle, the failure index corresponding to the cases of $\phi = 0^\circ$ and $\theta \neq 0^\circ$ would possess the values somewhat larger than those in the condition of $\theta = 0^\circ$ and $\phi \neq 0^\circ$, that is the extent of strength reduction for tower main-legs due to θ is usually more significant than that due to ϕ.

The stiffer the soil surrounding the base of the tower is the higher failure index in the main leg-members will usually be. Moreover, it is found that the variation tendencies of failure index are similar to those of the relative displacement at the top but not of the absolute displacement at the bottom of the main member.

References

AlBermani, F.G.A. and Kitipornchai, S. (1993), "Nonlinear finite element analysis of latticed transmission towers", *Eng. Struct.*, **15**, 259-269.

AlBermani, F.G.A. and Kitipornchai, S. (2003), "Numerical simulation of structural behavior of transmission towers", *Thin Wall. Struct.,* **41**, 167-177.

Desai, Y., Popplewell, N., Shah, A. and Buragohain, D. (1988) "Geometric nonlinear static analysis of cable supported structures", *Comput. Struct.*, **29**(8), 1001-1009.

Desai, Y., Yu, P., Popplewell, N. and Shah, A. (1995), "Finite element modelling of transmission line galloping", *Comput. Struct.*, **57**, 407-420.

Kitipornchai, S., AlBermani, F.G.A. and Peyrot, A.H. (1994), "Effect of bolt slippage on the ultimate strength of latticed structures", *J. Struct. Eng.*, **120**, 2281-2287.

Kitipornchai, S., Zhu, K., Xiang, Y. and AlBermani, F.G.A. (1991), "Single-equation yield surface for mono-symmetric and asymmetric sections", *Eng. Struct.*, **13**, 366-370.

Knight, G.M.S. and Santhakumar, A.R. (1993), "Joint effects on behavior of transmission towers", *J. Struct. Eng.*, **119**, 698-712.

Lei, Y.H. and Chien, Y.L. (2005) "Seismic analysis of transmission towers considering both geometric and material nonlinearities", *Tamkang J. Sci. Eng.*, **8**, 29-42.

Lei, Y.H. and Yeh, H.F. (2003), ìSeismic analysis for transmission towers with various line configuration-considering soil and structure interaction", *J. Chinese Inst. Civil Hydraulic Eng.*, **15**, 789-799.

Song, C. and Wolf, J.P. (1996), "Consistent infinitesimal finite-element-cell method: three-dimensional vector wave equation", *Int. J. Numer. Meth. Eng.*, **39**, 2189-2208.

Wolf, J.P. and Song, C. (1994), "Dynamic-stiffness matrix in time domain of unbounded medium by infinitesimal finite element cell method", *Earthq. Eng. Struct. Dyn.*, **23**, 1181-1198.

Wolf, J.P. and Song, C. (1997), *Finite-Element Modelling of Unbounded Media*, John Wiley & Sons, New York.

Appendix

$\mathbf{B}$	: strain-displacement relationship matrix of the element
$\mathbf{D}$	: stress-strain relationship matrix
$\mathbf{K}_e$	: elemental stiffness matrix of beam-column elements
$\mathbf{K}^*$	: mass matrix for finite-element cell
$\mathbf{M}^*$	: mass matrix for finite-element cell
$\mathbf{M}^{\infty}(t),_n$	: acceleration unit-impulse matrix cor-responding to nth time step (n = 1, 2,…, N)
$\mathbf{M}^{\infty}(t)$	: acceleration unit-impulse response matrix of far-field soil
$\mathbf{M}$, $\mathbf{C}$, $\mathbf{K}$	: global mass-, damping- and stiffness-matrices respectively
$\mathbf{p}(\omega)$	: nodal force acting on finite-element cell
$\underset{\sim}{\mathbf{S}}^{\infty}(\omega)$	: dynamic stiffness matrix of far-field soil
$\tilde{\mathbf{i}}$	: pseudo-static displacement vector of the system
$\mathbf{q}(t)$	: interaction forces acting on near-field soil
$\mathbf{r}(t)$	: interaction forces acting on far-field soil
$\mathbf{u}_i$	: nodal displacement vector
$\mathbf{u}(t)$	: displacement response vector of the system
A	: cross-sectional area of the element
E	: modulus of elasticity of the element
F_i	: nodal force of the element
G	: shear modulus of elasticity
J	: polar moment of inertia of beam-column element
L_c, L_e	: elemental lengths corresponding cable and beam-column elements
M_y	: flexural load for beam-column elements around y-axis
M_z	: flexural load for beam-column elements around z-axis
M_{py}, M_{pz}	: ultimate plastic moments of beam-column elements around y- and z-axes respectively
P	: axial force acting at beam-column elements
P_y	: axial yielding strength of beam-column elements
R_t	: axial stiffness coefficient related to bowing effect
S	: initial intrinsic coordinate of cable elements
S_{jy}, S_{jz}	: stability functions related to local y- and z-axes respectively
θ	: horizontal line-angle for tower system
Λ	: failure index of tower legs
λ	: input angle of seismic force
μ	: mass density of wires
ρ	: mass density of tower members
$\bar{r}$	: mass density of piles
$\tilde{\Phi}(p, m_x, m_y)$	: the function related to the yielding surface of the beam-column element in angle-section
ϕ	: vertical line-angle for tower system